

# A hybrid combinatorial-continuous strategy for solving molecular distance geometry problems\*

L. D. Secchin<sup>†</sup>    W. da Rocha<sup>‡</sup>    M. da Rosa<sup>‡</sup>    L. Liberti<sup>§</sup>    C. Lavor<sup>‡</sup>

October 24, 2025

## Abstract

The Molecular Distance Geometry Problem (MDGP) is essential in structural biology, as it seeks to determine three-dimensional protein structures from partial interatomic distances. Its discretizable subclass (DMDGP) admits an exact combinatorial formulation that enables efficient exploration of the search space. However, in practical settings such as Nuclear Magnetic Resonance (NMR) spectroscopy, distances are available only within uncertainty bounds, leading to the interval variant (*i*DMDGP). We propose a hybrid combinatorial–continuous framework for solving the *i*DMDGP. The method combines an enumeration process derived from the DMDGP with a continuous refinement stage that minimizes a nonconvex stress function that penalizes deviations from admissible distance intervals. This integration supports a systematic exploration guided by discrete structure and local optimization. The formulation incorporates torsion-angle intervals and chirality constraints through a refined atom ordering that preserves protein-backbone geometry. Numerical experiments show that the approach efficiently reconstructs geometrically valid conformations even under wide distance bounds, whereas most existing studies assume narrow ones.

**keywords:** Molecular Distance Geometry Problem, Spectral Projected Gradient Algorithm, 3D Protein Structure, Nuclear Magnetic Resonance

## 1 Introduction

The *Molecular Distance Geometry Problem* (MDGP) aims to determine the three-dimensional configuration of a protein molecule consistent with interatomic distance constraints from stereochemistry and Nuclear Magnetic Resonance (NMR) experiments. Typically, only a subset of pairwise distances is available [31].

Formally, let  $G = (V, E, d)$  be a weighted graph where  $V$  denotes atoms,  $E \subseteq V \times V$  the pairs with known distances, and  $d : E \rightarrow \mathbb{R}_{>0}$  assigns those distances. The MDGP asks for a realization  $x : V \rightarrow \mathbb{R}^3$  such that

$$\|x_u - x_v\| = d_{u,v}, \quad \forall \{u, v\} \in E,$$

with  $\|\cdot\|$  the Euclidean norm. A well-studied subclass, the *Discretizable* MDGP (DMDGP), is NP-hard [27, 31] yet exhibits rich combinatorial structure [29, 32]. Under an appropriate atom ordering and stereochemical constraints, the DMDGP search space can be represented by a binary search tree that can be explored by the *Branch-and-Prune* (BP) algorithm [30]. In this setting, the protein backbone geometry, parameterized by torsion angles  $\phi, \psi, \omega$  [16], is modeled using covalent bond lengths  $d_{i-1,i}$  and distances across two bonds  $d_{i-2,i}$  given *a priori* [37]. From NMR chemical shifts, approximate  $\phi, \psi$  values can be inferred [39], and typical  $\omega$  values are available in structural data [37], which can be converted into distances across three bonds ( $d_{i-3,i}$ ) [30], and completes the model.

To incorporate proximity information from NMR Nuclear Overhauser Effect *Spectroscopy* (NOESY) (long-range constraints between spatially close hydrogen atoms,  $< 5 \text{ \AA}$ ) [25], we include backbone-bound hydrogen atoms ( $H_N, H_\alpha$ ) together with  $N, C_\alpha$ , and  $C$ . Because this extension breaks the single-chain structure, we adopt an augmented atom ordering that allows repeated atoms and explicitly includes hydrogen atoms [26]. This ordering also guides BP exploration, since many hydrogen-related constraints span three or more bonds [13, 30].

\*This research was partially funded by the Brazilian research agencies FAPESP (grant numbers 2013/07375-0, 2022/06745-7, 2023/08706-1, 2024/00923-6, 2024/12967-8, 2024/15980-5, 2024/21786-7) and CNPq (grant numbers 305227/2022-0, 404616/2024-0, 302520/2025-2, 402609/2025-5).

<sup>†</sup>Departamento de Matemática Aplicada, Universidade Federal do Espírito Santo, ES, Brazil. [leonardo.secchin@ufes.br](mailto:leonardo.secchin@ufes.br)

<sup>‡</sup>Departamento de Matemática Aplicada, Universidade Estadual de Campinas, Campinas, SP, Brazil. [wdarocha@ime.unicamp.br](mailto:wdarocha@ime.unicamp.br), [marianadarosa13@gmail.com](mailto:marianadarosa13@gmail.com), [clavor@unicamp.br](mailto:clavor@unicamp.br)

<sup>§</sup>LIX CNRS, Ecole Polytechnique, Institut Polytechnique de Paris. [leo.liberti@polytechnique.edu](mailto:leo.liberti@polytechnique.edu)

Several alternative orderings exist, see *e.g.* [22, 31]. In our approach, we employ one that facilitates the representation of torsion angle intervals. Nevertheless, for didactic reasons and to avoid unnecessary technical detail, we adopt the well-established DMDGP ordering [27], which simplifies both the exposition and the theoretical development.

Uncertainties in NMR experiments motivate the interval variant (*i*DMDGP) [28], where each  $\{i, j\} \in E$  is associated with bounds  $[d_{i,j}^L, d_{i,j}^U]$  and one seeks  $x : V \rightarrow \mathbb{R}^3$  satisfying

$$d_{i,j}^L \leq \|x_i - x_j\| \leq d_{i,j}^U, \quad \forall \{i, j\} \in E.$$

Thus, the *i*DMDGP searches for a configuration  $X = [x_1, \dots, x_n] \in \mathbb{R}^{3 \times n}$  consistent with interval constraints, which is inherently more challenging than the exact case (from now on, if  $d_{i,j}^L = d_{i,j}^U$  we call  $d_{i,j}$  an *exact distance*; if  $d_{i,j}^L < d_{i,j}^U$ , we call it an *interval distance*).

To illustrate the *i*DMDGP, we consider a toy instance consisting of ten atoms. By definition, the distances  $d_{i-1,i}$ ,  $d_{i-2,i}$ ,  $d_{i-3,i}$  are specified for each admissible index  $i$  in the DMDGP ordering ( $4 \leq i \leq 10$ ). In this example, we additionally assume that NMR experiments detect interactions between the atom pairs  $\{1, 8\}$ ,  $\{2, 10\}$ , and  $\{3, 9\}$ , providing estimates for the corresponding interatomic distances. The distance matrix for this instance is organized as follows: the distances  $d_{i-1,i}$  and  $d_{i-2,i}$  are exact; all other experimentally determined entries (the “extra distances”) are given as intervals; and unknown entries are denoted by “?”, indicating pairs for which no measurement is available. For brevity, we display only the upper triangular part of the symmetric matrix:

$$\begin{bmatrix} 0 & d_{1,2} & d_{1,3} & [d_{1,4}^L, d_{1,4}^U] & ? & ? & ? & [d_{1,8}^L, d_{1,8}^U] & ? & ? \\ 0 & d_{2,3} & d_{2,4} & [d_{2,5}^L, d_{2,5}^U] & ? & ? & ? & ? & ? & [d_{2,10}^L, d_{2,10}^U] \\ 0 & d_{3,4} & d_{3,5} & [d_{3,6}^L, d_{3,6}^U] & ? & ? & ? & [d_{3,9}^L, d_{3,9}^U] & ? & ? \\ 0 & d_{4,5} & d_{4,6} & [d_{4,7}^L, d_{4,7}^U] & ? & ? & ? & ? & ? & ? \\ 0 & d_{5,6} & d_{5,7} & [d_{5,8}^L, d_{5,8}^U] & ? & ? & ? & [d_{6,9}^L, d_{6,9}^U] & ? & ? \\ 0 & d_{6,7} & d_{6,8} & [d_{7,8}^L, d_{7,8}^U] & ? & ? & ? & [d_{7,10}^L, d_{7,10}^U] & ? & ? \\ 0 & d_{7,8} & d_{7,9} & [d_{8,9}^L, d_{8,9}^U] & ? & ? & ? & [d_{8,10}^L, d_{8,10}^U] & ? & ? \\ 0 & d_{8,9} & d_{8,10} & [d_{9,10}^L, d_{9,10}^U] & ? & ? & ? & 0 & ? & ? \\ 0 & d_{9,10} & 0 & 0 & ? & ? & ? & ? & ? & ? \end{bmatrix}.$$

In most continuous approaches to distance-related problems [14, 19, 21], it is assumed that the distance intervals are narrow. In contrast, our framework considers a scenario closer to that observed in NMR experiments, where distance uncertainties are typically wider.

In this work we develop a *hybrid combinatorial-continuous* framework for the *i*DMDGP that integrates the enumerative strategy of [28] with a continuous formulation in the spirit of [20]. The method couples (i) an enumeration process based on the DMDGP search tree with (ii) a continuous optimization problem whose constraints measure violations of admissible intervals. This constitutes a practical step toward scalable hybrid algorithms for realistic *i*DMDGP instances.

## 2 Problem formulation and modeling assumptions

We summarize the modeling assumptions and notation used throughout the paper, postponing solver-dependent choices and placement formulas to Sections 3.1 and 4.

### Backbone geometry and atom ordering

We treat the protein backbone as a known sequence of residues with covalent bond lengths and bond angles fixed to standard values [16, 18]. Variability arises solely from torsion angles. Long-range interatomic distances (typically from NMR) are represented as intervals, whereas distances across one or two covalent bonds are considered exact.

To encode these relations, we adopt an *i*DMDGP ordering with repetitions of atoms, similar to [26], which allows us to explicitly include backbone-bound hydrogen atoms<sup>1</sup> ( $H_N$ ,  $H_\alpha$ ) and to couple torsion information with distance constraints through consecutive quadruples. This ordering is convenient for representing chirality and other orientation-dependent geometric properties, and it aligns with the discrete primitives used later (see Section 3.1).

<sup>1</sup>For proline, the peptide nitrogen is not bound to a hydrogen; we replace  $H_N^i$  by a  $\delta$ -hydrogen attached to  $C_\delta$ . For glycine, whose  $C_\alpha$  is bonded to two hydrogen atoms, only one is retained for modeling purposes.

## Torsion-angle domains and chirality

Let  $\tau_i$  denote the torsion angle associated with the  $i$ th quadruple of consecutive atoms in the ordering. Its feasible set is either a single interval,

$$\mathcal{T}_i = [\tau_i^L, \tau_i^U],$$

or the union of two symmetric intervals,

$$\mathcal{T}_i = [-\tau_i^U, -\tau_i^L] \cup [\tau_i^L, \tau_i^U],$$

depending on whether one or both orientations (signs) are admissible. We write  $\tau = (\tau_1, \dots, \tau_m) \in \mathcal{T}$  to indicate  $\tau_i \in \mathcal{T}_i$  for all  $i$ . In Section 3.1 we exploit the sign structure of  $\mathcal{T}_i$  to guide both construction and improvement steps while avoiding erratic side changes.

### 2.1 Distance data and optimization model

Let  $E$  be the set of pairs of atoms whose distances are known, each endowed with bounds  $[d_{i,j}^L, d_{i,j}^U]$ . A conformation  $X = [x_1 \dots x_n] \in \mathbb{R}^{3 \times n}$  is an *i*DMDGP solution if

$$d_{i,j}^L \leq \|x_i - x_j\| \leq d_{i,j}^U \quad \text{for all } \{i, j\} \in E. \quad (1)$$

To explicitly represent this experimental uncertainty within the model, we introduce auxiliary variables  $d = \{d_{i,j}\}_{\{i,j\} \in E}$  defined within the box

$$\Omega_d = \{d \mid d_{i,j}^L \leq d_{i,j} \leq d_{i,j}^U, \{i, j\} \in E\}.$$

This formulation separates (i) the misfit of  $\|x_i - x_j\|$  to the data from (ii) the enforcement of interval bounds, since projection onto  $\Omega_d$  is straightforward: for any real number  $r$ ,

$$d_{i,j} \leftarrow \Pi_{[d_{i,j}^L, d_{i,j}^U]}(r), \quad \Pi_{[a,b]}(r) := \min\{\max\{r, a\}, b\}.$$

In our setting,  $r$  is typically the current interatomic distance, i.e.,  $r = \|x_i - x_j\|$ .

Misfit to distance data is quantified by the (nonconvex) *stress* function

$$\sigma(X, d) = \frac{1}{2} \sum_{\{i,j\} \in E} w_{i,j} (\|x_i - x_j\| - d_{i,j})^2, \quad (2)$$

with positive weights  $w_{i,j}$  (Section 4 details our choices).

To determine a three-dimensional protein structure that is consistent with the distance constraints amounts to finding a conformation  $X$ , and distance variables  $d = \{d_{i,j}\}$ , such that the stress function  $\sigma(X, d)$  is zero and  $d$  satisfies the bounds, i.e.,  $d \in \Omega_d$ . Therefore, our optimization model is

$$\begin{aligned} \min_{X, d} \quad & \sigma(X, d) \\ \text{s.t.} \quad & d \in \Omega_d, \quad X \in \mathbb{R}^{3 \times n}. \end{aligned} \quad (3)$$

The function  $\sigma$  is smooth at any  $(X, d)$  with  $\|x_i - x_j\| > 0$ , for all  $\{i, j\} \in E$  [20], which makes it suitable for smooth optimization methods. Nevertheless, computing a global solution of (3) remains challenging due to its high-dimensional, nonconvex landscape. Consequently, practical continuous approaches often focus on generating high-quality initial conformations that can guide local optimization toward near-global minima.

**Practical notes.** A solution of (1) is invariant under rigid motions. In Section 3.1, we fix the first three atoms to remove this gauge freedom and describe how we (i) build angle-aware initial conformations, (ii) apply sign-consistent discrete improvements, and (iii) refine candidates for (3) via a projected-gradient scheme. Quality metrics (LDE/MDE) and stopping criteria are reported in Section 4.

## 3 Hybrid construction and optimization framework

### 3.1 Background and placement primitive

Generating a near-globally optimal conformation is challenging because  $\sigma$  is highly nonconvex. Two families of strategies are typically used to build good initial conformations from *a priori* information.

**(i) SDP-based models.** A common approach relies on semidefinite programming (SDP) relaxations for Euclidean distance matrix completion, with notable formulations in [2, 3, 4, 17]. These methods aim to find

low-rank realizations, ideally three-dimensional. However, they have limitations: (a) generating diverse initial conformations is not straightforward because the model is fixed; (b) only distance information is used, without explicit torsion-angle signs or chirality; and (c) solving large-scale SDP models for the interval case can be computationally demanding. Although facial reduction [17, 23] and low-rank formulations [6, 12] mitigate costs in the exact case, efficiency remains limited with interval data.

**(ii) Enumerative methods.** These exploit the discrete nature of the DMDGP by placing atoms sequentially and pruning infeasible branches. The *Branch-and-Prune* (BP) method [30] uses only distances; since the quartet  $(i-3, i-2, i-1, i)$  does not fix  $\tau_i$ , two symmetric placements for  $x_i$  arise, yielding a binary tree (Figure 1). An interval extension (iBP) [28] samples  $d_{i-3,i}$  within  $[d_{i-3,i}^L, d_{i-3,i}^U]$  and runs BP for each sample, which can grow combinatorially. To temper branching, [36] integrates local continuous optimization to adjust sampled  $d_{i-3,i}$  within their intervals; the MDJEEP package [35] applies Spectral Projected Gradient (SPG) method [9] to (3). Still, angular information is not used explicitly.

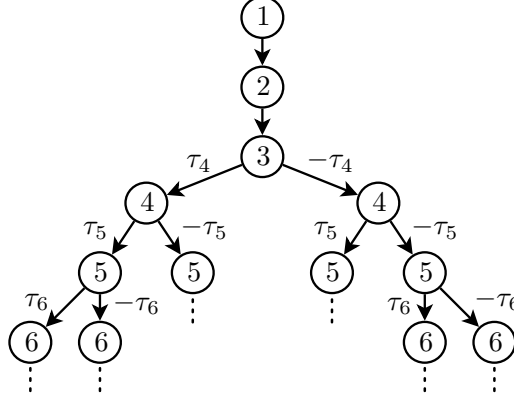


Figure 1: Enumerative search with exact distances. For  $i \geq 4$ , two symmetric placements correspond to the sign of  $\tau_i$ .

**Our stance.** Combinatorial and continuous views are complementary for the  $i$ DMDGP. We therefore combine (a) fast, angle-aware construction of conformations with (b) continuous refinement by SPG. The geometric placement primitive is as follows. We fix the first three atoms as

$$x_1 = \begin{bmatrix} 0 \\ 0 \\ 0 \end{bmatrix}, \quad x_2 = \begin{bmatrix} -d_{1,2} \\ 0 \\ 0 \end{bmatrix}, \quad x_3 = \begin{bmatrix} -d_{1,2} + d_{2,3} \cos \theta_3 \\ d_{2,3} \sin \theta_3 \\ 0 \end{bmatrix}, \quad (4)$$

where  $\theta_i$  is the bond angle at atom  $i$  (between  $i, i-1, i-2$ ), which satisfies the exact distances among atoms 1–3 [27]. Each subsequent atom  $i \geq 4$  is placed relative to its predecessors  $i-3, i-2, i-1$  as

$$x_i = x_{i-1} + U_i \begin{bmatrix} -d_{i-1,i} \cos \theta_i \\ d_{i-1,i} \sin \theta_i \cos \tau_i \\ d_{i-1,i} \sin \theta_i \sin \tau_i \end{bmatrix}, \quad (5)$$

where the columns of  $U_i$  are

$$u_1 = \frac{v_1}{\|v_1\|}, \quad u_2 = \frac{v_1 \times v_2}{\|v_1 \times v_2\|}, \quad u_3 = u_2 \times u_1, \quad (6)$$

with  $v_1 = x_{i-1} - x_{i-2}$  and  $v_2 = x_{i-3} - x_{i-2}$  [22]. After computing  $x_i$ , we check all long-range distances  $d_{j,i}$  ( $j < i-3$ ) and prune infeasible branches. This primitive underlies the three algorithms in Section 3.2.1–3.2.3.

## 3.2 Algorithms

Our procedure unfolds in three phases. *Algorithm 1* builds an angle-aware initial conformation by sampling torsions within their admissible sets and selecting the placement that minimizes a local distance error (LDE). *Algorithm 2* performs a discrete neighborhood search by flipping torsion signs whenever both orientations are admissible, restricting subsequent samples to the sign-consistent portion of each torsion domain; only improving flips (in terms of global LDE) are accepted. *Algorithm 3* orchestrates multistart runs of Algorithms 1–2, filters near-duplicates via an RMSD threshold, and refines selected candidates by SPG on the continuous model (3) with projected distance variables. Early stopping is triggered as soon as either LDE or MDE meets the prescribed tolerance.

The choice of SPG over other optimization methods in the refinement phase is motivated by its low computational cost: no system needs to be solved, only first-order derivatives are required and memory requirements are minimal, making it well suited for large-scale problems such as (3). Furthermore, it has been shown to effectively minimize general highly nonconvex functions [8], such as (2), up to a moderate accuracy across a wide range of applications; see [11, 40] and references therein. In particular, SPG was considered in the context of MDGP [21, 35, 36].

### 3.2.1 Algorithm 1 — Angle-guided greedy construction

Algorithm 1 produces a fast, chirality-aware initialization that is consistent with discretization distances up to numerical precision. For each atom  $i$ , it samples  $\tau_i$  within its admissible domain and selects the trial that yields the smallest local inconsistency (LDE $_i$ ) with already placed atoms. This local criterion is inexpensive and tends to propagate feasible geometry forward while respecting torsion-angle signs.

---

#### Algorithm 1 GREEDY\_CONSTRUCTION( $N_{\text{tors}}$ , $\mathcal{T}$ )

---

```

1: Set  $x_1$ ,  $x_2$  and  $x_3$  as in (4)
2: for  $i = 4, \dots, n$  do
3:    $\text{BEST\_LDE}_i \leftarrow \infty$ 
4:   for  $t = 1, \dots, N_{\text{tors}}$  do
5:     Sample  $\tau_i \in \mathcal{T}$ 
6:     Place  $x_i$  using (5)–(6)
7:     if  $\text{LDE}_i(x_1, \dots, x_i) < \text{BEST\_LDE}_i$  then
8:        $\text{BEST\_LDE}_i \leftarrow \text{LDE}_i(x_1, \dots, x_i)$ 
9:        $\text{BEST\_TORSION}_i \leftarrow \tau_i$ 
10:       $\tau_i \leftarrow \text{BEST\_TORSION}_i$ 
11:    Compute  $X = [x_1, \dots, x_n]$  from  $\tau$ 
12:  return  $\tau$  and  $X \in \mathbb{R}^{3 \times n}$ 

```

---

Here

$$\text{LDE}_i(X) = \max_{\{i,j\} \in E, i > j} \left\{ 0, \frac{d_{i,j}^L - \|x_i - x_j\|}{d_{i,j}^L}, \frac{\|x_i - x_j\| - d_{i,j}^U}{d_{i,j}^U} \right\}.$$

**Global metrics.** For a given conformation  $X$ , define for each edge  $\{i, j\} \in E$  the normalized residual

$$\delta_{i,j}(X) = \max \left\{ 0, \frac{d_{i,j}^L - \|x_i - x_j\|}{d_{i,j}^L}, \frac{\|x_i - x_j\| - d_{i,j}^U}{d_{i,j}^U} \right\}.$$

From  $\delta_{i,j}(X)$ , we consider the global metrics

$$\text{LDE}(X) := \max_{\{i,j\} \in E} \delta_{i,j}(X) \quad \text{and} \quad \text{MDE}(X) := \frac{1}{|E|} \sum_{\{i,j\} \in E} \delta_{i,j}(X).$$

For exact distances ( $d_{i,j}^L = d_{i,j}^U = d_{i,j}$ ) one has  $\delta_{i,j}(X) = \|\|x_i - x_j\| - d_{i,j}\|/d_{i,j}$ ; for interval distances,  $\delta_{i,j}(X) = 0$  whenever  $\|x_i - x_j\| \in [d_{i,j}^L, d_{i,j}^U]$ . These quantities are used in the tolerance thresholds  $\varepsilon_{\text{LDE}}$  and  $\varepsilon_{\text{MDE}}$  in Algorithm 3.

### 3.2.2 Algorithm 2 — Sign-consistent local improvement

The second phase explores discrete alternatives by flipping torsion signs when both orientations are admissible. To avoid erratic side changes, new trials restrict  $\tau_i$  to the portion of  $\mathcal{T}_i$  consistent with the chosen sign:

$$\mathcal{T}_i^{\text{sgn}}(\tau) = \begin{cases} \mathcal{T}_i \cap [0, \infty) & \text{if } \tau > 0, \\ \mathcal{T}_i \cap (-\infty, 0] & \text{if } \tau < 0. \end{cases}$$

For each  $i$ , we flip the sign (if allowed), rebuild a trial conformation with Algorithm 1 using  $\mathcal{T}_i^{\text{sgn}}$ , and keep the change only if it improves the total LDE. This targeted move often repairs mismatches introduced by purely local choices in Algorithm 1 without incurring a combinatorial blow-up.

---

**Algorithm 2** IMPROVE( $X, \tau, N_{\text{tors}}$ )

---

```

1: for  $i = 4, \dots, n$  do
2:    $\tau^{\text{trial}} \leftarrow \tau$ 
3:   if  $-\tau_i^{\text{trial}} \in \mathcal{T}_i$  then ▷ both orientations admissible
4:      $\tau_i^{\text{trial}} \leftarrow -\tau_i^{\text{trial}}$ 
5:      $\mathcal{T}_i^{\text{trial}} \leftarrow \mathcal{T}_i^{\text{sgn}}(\tau_i^{\text{trial}})$ 
6:      $\tau^{\text{trial}}, X^{\text{trial}} = \text{GREEDY\_CONSTRUCTION}(N_{\text{tors}}, \mathcal{T}_i^{\text{trial}})$ 
7:     if  $\text{LDE}(X^{\text{trial}}) < \text{LDE}(X)$  then
8:        $X \leftarrow X^{\text{trial}}; \tau \leftarrow \tau^{\text{trial}}$ 

```

---

### 3.2.3 Algorithm 3 — Multistart orchestration (Alg. 1+2) and SPG refinement

Algorithm 3 diversifies initializations (via multistart of Algorithms 1–2), discards near-duplicates based on RMSD, and then performs continuous refinement by SPG on (3). Distance auxiliaries  $d_{ij}$  are initialized by projecting the current interatomic distances onto their admissible intervals  $[d_{ij}^L, d_{ij}^U]$ , yielding a good starting point for the SPG method applied to problem (3).

Termination occurs either when the MDE or LDE tolerances are satisfied or when the budget of distinct conformations is exhausted.

**Similarity filter (RMSD).** We measure similarity between two conformations  $X$  and  $Y$  via the Kabsch-aligned RMSD:

$$\text{RMSD}(X, Y) = \min_{Q \in \mathbb{R}^{3 \times 3}, Q^\top Q = I} \frac{1}{\sqrt{n}} \| \tilde{Y} - \tilde{X}Q \|_F,$$

where  $\| \cdot \|_F$  is the Frobenius norm,  $Q$  is orthogonal (Kabsch alignment) [24], and  $\tilde{X}, \tilde{Y}$  are centralized at the same center of mass. For  $n \leq 200$  we use all atoms; otherwise, only the  $C_\alpha$  subset [1]. Candidates with  $\text{RMSD} \leq \varepsilon_{\text{similar}}$  are treated as near-duplicates and skipped.

---

**Algorithm 3** Multistart orchestration (Alg. 1+2) with SPG refinement

---

**Initialization.** Set parameters:

- $N_{\text{trial}} > 0$ : maximum number of trials
- $N_{\text{conf}} > 0$ : maximum number of distinct initial conformations
- $N_{\text{tors}} \geq 0$ : trials per atom in GREEDY\_CONSTRUCTION
- $N_{\text{impr}} > 0$ : repetitions of IMPROVE
- $\varepsilon_{\text{MDE}} > 0, \varepsilon_{\text{LDE}} > 0$ : feasibility tolerances
- $\varepsilon_{\text{similar}} > 0$ : RMSD threshold to declare conformations “equal”

Initialize the pool  $C \leftarrow \emptyset$

```

1: for  $c = 1, \dots, N_{\text{trial}}$  do
2:    $\tau^c, X^c = \text{GREEDY\_CONSTRUCTION}(N_{\text{tors}}, \mathcal{T})$  ▷ Algorithm 1
3:   for  $t = 1, \dots, N_{\text{impr}}$  do
4:     IMPROVE( $X^c, \tau^c, N_{\text{tors}}$ ) ▷ Algorithm 2
5:     if  $\text{MDE}(X^c) \leq \varepsilon_{\text{MDE}}$  or  $\text{LDE}(X^c) \leq \varepsilon_{\text{LDE}}$  then return  $X^c$ 
6:     if  $\exists X^j \in C$  s.t.  $\text{RMSD}(X^c, X^j) \leq \varepsilon_{\text{similar}}$  then continue
7:     Set  $d_{i,j} \leftarrow \Pi_{[d_{i,j}^L, d_{i,j}^U]}(\|x_i - x_j\|)$  for each  $\{i, j\} \in E$ , where  $[x_1, \dots, x_n] = X^c$ 
8:     Apply SPG to (3) starting from  $(X^c, d)$ 
9:     if  $\text{MDE}(X^c) \leq \varepsilon_{\text{MDE}}$  or  $\text{LDE}(X^c) \leq \varepsilon_{\text{LDE}}$  then return  $X^c$ 
10:     $C \leftarrow C \cup \{X^c\}$ 
11:    if  $|C| > N_{\text{conf}}$  then break
12: return the conformation with the smallest MDE found so far

```

---

Since the multistart strategy explores different initialization paths, several distinct conformations can be generated during the search. Each conformation corresponds to a locally optimized structure obtained after refinement. The best conformation found is defined as the one achieving the smallest MDE value among all conformations generated within the computational budget.

## 4 Computational results

### 4.1 Experimental setup and parameters

We implemented all algorithms in **Julia** and ran the experiments in single-threaded mode on an AMD Threadripper 1950X with 64 GB RAM under Ubuntu 22.04.5 LTS. Source code is available at <https://github.com/leonardosecchin/MDGP>.

All weights  $w_{ij}$  in (2) are set equal, except those associated with discretization distances, which are doubled to preserve, as much as possible, the satisfaction achieved in the construction phase after applying SPG; the weight vector is then normalized.

In Algorithm 3, we declare a “success” if, in line 8 of the SPG phase, the stress function value reaches at most  $10^{-7}$ , or if the stopping criteria in Algorithm 3 are met.

We cap SPG at 30,000 iterations per conformation and also adopt a lack-of-progress stop: termination occurs when the step length becomes numerically zero or the relative decrease in stress is insufficient for 100 consecutive iterations. In practice, SPG typically halts well before the iteration cap; hence, “failure” corresponds to stalling at a nonoptimal local minimum. SPG parameters follow [9]:  $\gamma = 10^{-4}$ ,  $m = 10$ ,  $\lambda_{\min} = 10^{-30}$ ,  $\lambda_{\max} = 10^{30}$ ,  $\sigma_1 = 0.1$ ,  $\sigma_2 = 0.9$ ; the initial spectral step is computed as in [10].

For Algorithm 3 we use  $N_{\text{trial}} = 500$ ,  $N_{\text{conf}} = 50$ ,  $N_{\text{tors}} = 20$ ,  $N_{\text{impr}} = 3$ ,  $\varepsilon_{\text{MDE}} = 10^{-3}$ ,  $\varepsilon_{\text{LDE}} = 10^{-2}$ , and  $\varepsilon_{\text{similar}} = 5.0$ . We also stop generating new conformations if, for 50 consecutive trials, no conformation different from the previous ones (in the sense of line 6) is found.

### 4.2 Computational experiments

We compare Algorithm 3 against MDJEEP [35], since both combine enumerative ideas with a continuous minimization step and MDJEEP is a well-established baseline for the setting considered. We use the parameters suggested in the example provided in its repository <https://github.com/mucherino/mdjeep>.

The benchmark set comprises 30 instances, ranging from 87 atoms (17 residues) to 1,347 atoms (269 residues), derived from PDB structures [7]. Each instance is constructed by considering angular intervals of width  $50^\circ$  [34] for  $\phi$  and  $\psi$  torsion angles, and distance constraints of width 1 Å between hydrogen atoms belonging to adjacent residues or 2 Å otherwise [38]. The hydrogen–hydrogen distance constraints are computed exclusively between atoms located within 5 Å in the reference structure. The maximum CPU time for Algorithm 3 and MDJEEP was set to 5 hours. It is worth noting that runtimes smaller than 1 second were considered equal to 1 (in such case, natural fluctuations in the computation of CPU times make the comparison meaningless). Results are summarized in Table 1. Column  $N_c$  reports the number of conformations produced by Algorithm 3 until termination. All percentages were rounded to the nearest integer to simplify the presentation of results.

**Runtime behavior.** Within the time limit, MDJEEP solves 60% of the instances, whereas Algorithm 3 solves 77% and does so in markedly smaller runtimes. The runtime of MDJEEP varies substantially even for instances of similar size. Enumerative search is highly sensitive to long-range constraints appearing late in the ordering: infeasibilities discovered near the bottom of the tree trigger large reconstructions. Moreover, early inaccurate samples can cascade through the tree, forcing many retries. Our hybrid strategy is less sensitive to these effects: once an initial (possibly infeasible) conformation is built, we optimize it as a whole. Overall runtime depends more on the number of distinct conformations generated before convergence, often small ( $\leq 5$ ), than on the raw number of atoms/distances. This suggests that Algorithms 1 and 2 jointly provide strong initializations for SPG.

**Role of continuous refinement.** Continuous local optimization is essential. MDJEEP consistently handles instances up to 252 atoms (about 92% of them), which would be unlikely for purely enumerative methods with wide intervals. Similarly, removing SPG from Algorithm 3 (omitting lines 7–8) produces a dramatic loss in robustness. In short, the approach is ineffective without the refinement step via optimization of (3).

### 4.3 Performance profiles and ablation

We present the results in terms of performance profiles [15] (see Figure 2), a widely used tool in the optimization community to compare efficiency and robustness of algorithms. Let us briefly explain how they work. Consider

Table 1: Computational results. Times are in seconds; best values in bold. Italic values for Algorithm 3 indicate that the prescribed tolerances were not met; in this case, we report the conformation with the smallest MDE. “–” indicates that the algorithm does not converge within 5 hours.

ID	n	E	Algorithm 3				MDJEEP		
			$N_c$	LDE	MDE	time	LDE	MDE	time
1EQQ	87	363	1	1.05e-02	9.88e-04	< <b>1.00</b>	3.77e-03	3.30e-04	2.00
1H07	102	485	1	9.86e-03	1.13e-03	< <b>1.00</b>	4.20e-03	2.56e-04	<b>1.00</b>
1LFC	127	562	1	1.04e-02	9.98e-04	< <b>1.00</b>	5.87e-03	3.85e-04	175.51
1MMC	152	702	1	2.08e-02	1.00e-03	< <b>1.00</b>	2.43e-02	4.72e-04	1,094.10
6HKA	165	759	1	2.35e-02	9.86e-04	< <b>1.00</b>	1.19e-02	4.86e-04	6.78
1SPF	177	836	1	3.91e-02	9.88e-04	< <b>1.00</b>	1.03e-02	3.59e-04	3.36
1C56	202	942	3	2.16e-02	9.99e-04	<b>1.24</b>	1.02e-02	4.67e-04	119.00
2LKS	220	1,017	1	4.11e-02	9.90e-04	< <b>1.00</b>	1.80e-02	4.65e-04	2.16
7EAU	245	1,121	3	2.79e-02	9.99e-04	<b>3.83</b>	1.08e-02	4.75e-04	1,089.32
6QBK	247	1,151	7	3.82e-02	1.00e-03	<b>9.17</b>	—	—	—
2KNX	252	1,150	2	1.91e-02	1.00e-03	<b>2.03</b>	1.39e-02	4.14e-04	137.00
7PQW	252	1,156	14	3.71e-02	1.00e-03	<b>18.49</b>	7.83e-03	4.65e-04	2,875.26
2EGE	375	1,688	50	2.56e-02	1.00e-03	103.80	—	—	—
2YRT	375	1,732	5	3.02e-02	1.00e-03	<b>5.17</b>	2.30e-02	4.49e-04	11,375.00
2KW9	377	1,656	1	5.61e-02	9.99e-04	< <b>1.00</b>	1.48e-02	4.77e-04	27.00
1KCY	377	1,838	6	3.09e-02	9.99e-04	<b>12.66</b>	1.62e-02	3.74e-04	3,779.00
2N2N	475	2,302	17	7.46e-02	1.00e-03	<b>36.76</b>	—	—	—
2N9D	475	2,318	5	3.31e-02	1.00e-03	<b>6.04</b>	—	—	—
2EBT	500	2,216	2	4.61e-02	1.00e-03	< <b>1.00</b>	2.01e-02	4.97e-04	44.74
1JOF	500	2,358	30	3.28e-02	1.00e-03	<b>57.62</b>	—	—	—
8VRC	500	2,362	8	2.55e-02	9.94e-04	<b>18.81</b>	1.95e-02	4.16e-04	4,010.00
2VB5	502	2,268	50	5.10e-02	1.06e-03	149.46	—	—	—
2J4M	502	2,309	5	6.45e-02	1.00e-03	<b>9.92</b>	1.09e-02	4.27e-04	5,214.00
1DX0	520	2,424	1	4.07e-02	1.00e-03	<b>1.80</b>	1.55e-02	3.98e-04	933.72
1A66	892	4,023	50	4.59e-02	1.70e-03	213.66	—	—	—
1BC9	1,002	4,674	22	6.75e-02	1.00e-03	<b>97.41</b>	—	—	—
1JCU	1,042	4,774	50	5.93e-02	1.71e-03	219.95	—	—	—
1AP8	1,067	5,047	50	7.94e-02	1.93e-03	169.29	—	—	—
1EZA	1,297	6,138	50	4.99e-02	1.29e-03	342.34	—	—	—
1AH2	1,347	6,427	50	8.41e-02	3.65e-03	267.04	—	—	—

the set  $P$  of all instances (in our case, 1E0Q, 1H07, 1LFC, etc.) and an algorithm  $a$ . The performance profile (for the algorithm  $a$ ) is the plot of the function  $\rho_a : [1, \infty) \rightarrow [0, 1]$  defined by

$$\rho_a(t) = \frac{1}{|P|} \text{card}\{p \in P \mid r_{p,a} \leq t\}, \quad r_{p,a} = \frac{\text{runtime of algorithm } a \text{ on } p}{\text{minimum runtime among all algorithms on } p},$$

where “card” stands for the cardinality of a set. The expression  $r_{p,a} = R \geq 1$  means that “algorithm  $a$  takes  $R$  times the runtime of the fastest algorithm on  $p$ ”. So,  $\rho_a(t)$  is the percentage of problems solved by algorithm  $a$  in *at most*  $t$  times the runtime of the fastest algorithm.

**Two useful reading points.** (i) At  $t = 1$  (left edge),  $\rho_a(1)$  is the fraction of problems on which  $a$  is the *fastest*; this quantifies *efficiency*. (ii) For an intermediate value of  $t$ , let us say for example  $t = 2^4 = 16$ ,  $\rho_a(16)$  is the fraction of problems  $a$  solves within at most sixteen times the best runtime (note that the  $x$ -axis in Figure 2 is shown on a  $\log_2$  scale for better visualization of performance ratios). In this case, MDjeep and Algorithm 3 solved 18% and 75% of the problems, respectively. Reading the curve at these abscissas provides complementary views: the left side reflects how often  $a$  wins outright; points to the right indicate how tolerant one must be (in runtime multiples) to obtain a given coverage of solved instances. When an algorithm  $a$  does not solve  $p$ , its runtime is defined as  $\infty$ ; then  $r_{p,a} = \infty$  (by convention,  $r_{p,a} = \infty$  also when “ $\infty/\infty$ ” occurs). This is the case of 1A66 for both algorithms. With this,  $\rho_a(t)$  for large  $t$  gives the number of problems solved by  $a$  essentially “independently” of its runtime (*i.e.*, *robustness*). In this sense, performance profiles balance efficiency (near  $t = 1$ ) and robustness (large  $t$ ). It is worth noting that runtimes smaller than 1 second were set to 1 (as in Table 1); in such cases, natural fluctuations in measured CPU times make a finer comparison meaningless. Figure 2 shows that, under the 5-hour cap, MDJEEP needs more than  $2^{11} = 2,048$  times the runtime of Algorithm 3 to reach its maximum robustness on the instances considered.

**Ablation: impact of sign-consistent improvement.** We measure the performance of Algorithm 3 without the improvement step (Algorithm 2), which corresponds to setting  $N_{\text{impr}} = 0$  (*i.e.*, conformations are computed solely with Algorithm 1). For a fair comparison, we set  $N_{\text{tors}} = 60$  so that the total number of torsion trials is comparable to the regular algorithm. The two variants are similarly efficient (about 53% vs. 57% fastest cases, read at  $t = 1$ ), but the full algorithm solves more problems overall (77% vs. 67%, read on the right side of the profiles). Its performance profile dominates from  $t \approx 2^0 = 1$ , indicating that sign-consistent flips improve robustness without harming efficiency.

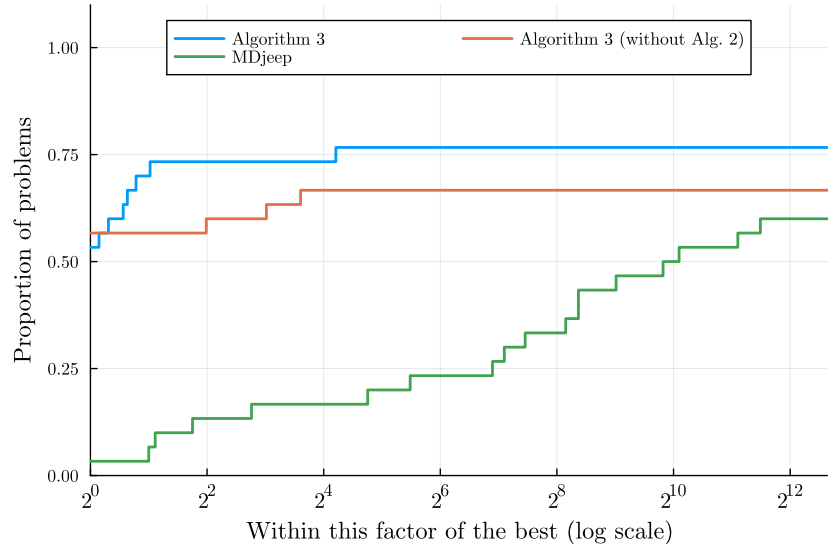


Figure 2: Runtime performance profiles among all instances (x-axis in  $\log_2$  scale).

## 5 Final remarks

We proposed a hybrid combinatorial–continuous framework for the *i*DMDGP in protein backbone reconstruction from NMR data. The approach couples (i) an angle-guided greedy construction, (ii) a sign-consistent discrete improvement, and (iii) multistart orchestration with spectral projected gradient (SPG) refinement. By injecting torsion-angle interval information into an enumerative placement and then applying continuous optimization, the method balances discrete exploration with local refinement.

**Historical context and trade-offs.** Early solution strategies for MDGP were primarily based on continuous optimization (see, for example, [14, 19, 20]). Such methods scale well, are flexible to noisy data, and can incorporate diverse penalties, but they do not provide a principled way to *systematically explore* the full search space and may stall at suboptimal local minima. In contrast, the discretizable subclass (DMDGP) admits an enumerative treatment [27], which can (in principle) exhaustively traverse the discrete search space under exact-distance assumptions, ensuring completeness on that model class. The cost is potential combinatorial blow-up and sensitivity to late-appearing constraints. Each paradigm has clear strengths and limitations; combining them is natural. Our results support this view: discrete structure sharply narrows the search, while continuous refinement reconciles interval data and mitigates local traps.

**Significance for NMR-based structure determination.** In NMR, distances are indirect and often reflect time-averaged interactions over conformational ensembles rather than a single static structure. NOESY-derived bounds, in particular, are affected by motional averaging and experimental uncertainty, leading to intervals that may be substantially wider than X-ray-based restraints [25]. Methods that remain effective under wide bounds and heterogeneous constraints are therefore useful. Our framework addresses this need by using distance geometry to constrain placements to chemically plausible regions and continuous optimization to reconcile all interval restraints at the conformation level. In practice, the multistart mechanism yields a pool of diverse candidates that can be clustered into conformational sub-states (via RMSD), aligning with ensemble interpretations common in NMR analysis.

**Discrete–continuous synergy.** The experiments highlight a general principle: discrete structure and continuous optimization are complementary for inverse problems in distance geometry. The discretization (ordering, pruning, sign logic) encodes chirality and backbone geometry and reduces the feasible region; the continuous stage provides robustness to noise and exploits all interval information jointly. This division of labor mitigates the combinatorial growth typical of purely enumerative strategies and reduces runtime variability caused by late-violated constraints.

**Summary of empirical findings.** On a benchmark of 30 protein instances (87–1,347 atoms), the method solved a larger fraction of problems than the MDJEEP baseline under the same 5-hour cap (77% vs. 60%) and did so with shorter runtimes. Ablation experiments indicate that sign-consistent flips improve robustness without degrading efficiency, and that the SPG stage is necessary to reach embeddings that satisfy LDE/MDE tolerances. These findings support the claim that seeding continuous refinement with torsion-aware discrete construction is effective under wide distance intervals.

**Future work.** Our initialization samples torsions uniformly, which does not reflect the statistics of real proteins. Because Algorithm 1 is modular (line 5), it can incorporate priors from Ramachandran maps or PDB-derived distributions [33]. A second direction is to enforce van der Waals lower bounds, either as additional intervals or in a dedicated stage; while this increases the number of stress terms, scalable updates (*e.g.*, stochastic or block-coordinate) [5] can limit overhead, or van der Waals checks can be deferred to post-processing. Finally, ensemble-aware formulations that optimize multiple conformations against time-averaged restraints and relaxation-derived constraints would better capture protein dynamics; this can be integrated into our framework by refining a small set of diverse conformers from the multistart pool with shared interval objectives and mild regularization toward diversity.

In summary, explicitly combining distance geometry with continuous optimization yields a practical and scalable solver for realistic *i*DMDGP instances, accommodating the wide and uncertain restraints typical of NMR. The hybrid route leverages the complementary advantages of completeness-oriented discrete search and robustness-oriented continuous refinement, and it appears to be a promising direction for distance-geometry problems with experimental uncertainty.

## Acknowledgements

This research was partially funded by the Brazilian research agencies FAPESP (grant numbers 2013/07375-0, 2022/06745-7, 2023/08706-1, 2024/00923-6, 2024/12967-8, 2024/15980-5, 2024/21786-7) and CNPq (grant numbers 305227/2022-0, 404616/2024-0, 302520/2025-2, 402609/2025-5). We would also like to thank Dr. Marcos Raydan, from the Universidade Nova de Lisboa, for the fruitful discussions on all the ideas in the paper during the period when CL and MR visited it in the 1st half of 2025.

## Declarations

**Conflict of interest.** The authors declare no conflict of interest.

## References

- [1] I. Aier, P. K. Varadwaj, and U. Raj. Structural insights into conformational stability of both wild-type and mutant EZH2 receptor. *Scientific Reports*, 6(1), oct 2016. [doi:10.1038/srep34984](https://doi.org/10.1038/srep34984).
- [2] S. Al-Homidan and H. Wolkowicz. Approximate and exact completion problems for Euclidean distance matrices using semidefinite programming. *Linear Algebra and its Applications*, 406:109–141, sep 2005. [doi:10.1016/j.laa.2005.03.021](https://doi.org/10.1016/j.laa.2005.03.021).
- [3] A. Y. Alfakih, A. Khandani, and H. Wolkowicz. Solving Euclidean distance matrix completion problems via semidefinite programming. *Computational Optimization and Applications*, 12:13–30, 1999. [doi:10.1023/A:1008655427845](https://doi.org/10.1023/A:1008655427845).
- [4] B. Alipanahi, N. Krislock, A. Ghodsi, H. Wolkowicz, L. Donaldson, and M. Li. Determining protein structures from NOESY distance constraints by semidefinite programming. *Journal of Computational Biology*, 20:296–310, apr 2013. [doi:10.1089/cmb.2012.0089](https://doi.org/10.1089/cmb.2012.0089).
- [5] V. S. Amaral, R. Andreani, E. G. Birgin, D. S. Marcondes, and J. M. Martínez. On complexity and convergence of high-order coordinate descent algorithms for smooth nonconvex box-constrained minimization. *Journal of Global Optimization*, 84:527–561, apr 2022. [doi:10.1007/s10898-022-01168-6](https://doi.org/10.1007/s10898-022-01168-6).
- [6] S. Bellavia, J. Gondzio, and M. Porcelli. A relaxed interior point method for low-rank semidefinite programming problems with applications to matrix completion. *Journal of Scientific Computing*, 89(2), oct 2021. [doi:10.1007/s10915-021-01654-1](https://doi.org/10.1007/s10915-021-01654-1).
- [7] H. M. Berman, J. Westbrook, Z. Feng, G. Gilliland, T. N. Bhat, H. Weissig, I. N. Shindyalov, and P. E. Bourne. The protein data bank. *Nucleic Acids Res.*, 28(1):235–242, 2000. [doi:10.1093/nar/28.1.235](https://doi.org/10.1093/nar/28.1.235).
- [8] E. G. Birgin, J. M. Martínez, and M. Raydan. Nonmonotone spectral projected gradient methods on convex sets. *SIAM Journal on Optimization*, 10:1196–1211, 2000.
- [9] E. G. Birgin, J. M. Martínez, and M. Raydan. Algorithm 813: SPG-software for convex-constrained optimization. *ACM Transactions on Mathematical Software*, 27:340–349, 2001. [doi:10.1145/502800.502803](https://doi.org/10.1145/502800.502803).
- [10] E. G. Birgin, J. M. Martínez, and M. Raydan. Inexact spectral projected gradient methods on convex sets. *IMA Journal of Numerical Analysis*, 23(4):539–559, 2003. [doi:10.1093/imanum/23.4.539](https://doi.org/10.1093/imanum/23.4.539).
- [11] E. G. Birgin, J. M. Martínez, and M. Raydan. Spectral projected gradient methods: Review and perspectives. *Journal of Statistical Software*, 60(3):1–21, 2014. [doi:10.18637/jss.v060.i03](https://doi.org/10.18637/jss.v060.i03).
- [12] S. Burer and R. D. Monteiro. A nonlinear programming algorithm for solving semidefinite programs via low-rank factorization. *Mathematical Programming*, 95(2):329–357, feb 2003. [doi:10.1007/s10107-002-0352-8](https://doi.org/10.1007/s10107-002-0352-8).
- [13] R. Carvalho, C. Lavor, and F. Protti. Extending the geometric build-up algorithm for the molecular distance geometry problem. *Information Processing Letters*, 108:234–237, 2008. [doi:10.1016/j.ipl.2008.05.009](https://doi.org/10.1016/j.ipl.2008.05.009).
- [14] I. Dokmanic, R. Parhizkar, J. Ranieri, and M. Vetterli. Euclidean distance matrices: Essential theory, algorithms, and applications. *IEEE Signal Processing Magazine*, 32:12–30, nov 2015. [doi:10.1109/MSP.2015.2398954](https://doi.org/10.1109/MSP.2015.2398954).
- [15] E. D. Dolan and J. J. Moré. Benchmarking optimization software with performance profiles. *Mathematical Programming*, 91(2):201–213, 2002. [doi:10.1007/s101070100263](https://doi.org/10.1007/s101070100263).
- [16] B. R. Donald. *Algorithms in Structural Molecular Biology*. MIT Press, 2011.
- [17] D. Drusvyatskiy, N. Krislock, Y.-L. Voronin, and H. Wolkowicz. Noisy euclidean distance realization: Robust facial reduction and the Pareto frontier. *SIAM Journal on Optimization*, 27(4):2301–2331, jan 2017. [doi:10.1137/15m103710x](https://doi.org/10.1137/15m103710x).

[18] R. A. Engh and R. Huber. Accurate bond and angle parameters for X-ray protein structure refinement. *Acta Crystallographica Section A Foundations of Crystallography*, 47(4):392–400, jul 1991. [doi:10.1107/s0108767391001071](https://doi.org/10.1107/s0108767391001071).

[19] H.-r. Fang and D. P. O’Leary. Euclidean distance matrix completion problems. *Optimization Methods and Software*, 27:695–717, oct 2012. [doi:10.1080/10556788.2011.643888](https://doi.org/10.1080/10556788.2011.643888).

[20] W. Glunt, T. Hayden, and M. Raydan. Molecular conformations from distance matrices. *Journal of Computational Chemistry*, 14:114–120, jan 1993. [doi:10.1002/jcc.540140115](https://doi.org/10.1002/jcc.540140115).

[21] D. S. Gonçalves and A. Mucherino. A distance geometry procedure using the Levenberg-Marquardt algorithm and with applications in biology but not only. In *Bioinformatics and Biomedical Engineering*, pages 142–152, Cham, 2022. Springer International Publishing. [doi:10.1007/978-3-031-07802-6\\_13](https://doi.org/10.1007/978-3-031-07802-6_13).

[22] D. S. Gonçalves and A. Mucherino. Discretization orders and efficient computation of cartesian coordinates for distance geometry. *Optimization Letters*, 8(7):2111–2125, feb 2014. [doi:10.1007/s11590-014-0724-z](https://doi.org/10.1007/s11590-014-0724-z).

[23] S. Huang and H. Wolkowicz. Low-rank matrix completion using nuclear norm minimization and facial reduction. *Journal of Global Optimization*, 72(1):5–26, nov 2017. [doi:10.1007/s10898-017-0590-1](https://doi.org/10.1007/s10898-017-0590-1).

[24] W. Kabsch. A solution for the best rotation to relate two sets of vectors. *Acta Crystallographica Section A*, 32(5):922–923, 1976. [doi:10.1107/S0567739476001873](https://doi.org/10.1107/S0567739476001873).

[25] W. Kurt. *NMR of Proteins and Nucleic Acids*. Wiley, New York, 1986.

[26] C. Lavor, L. Liberti, B. Donald, B. Worley, B. Bardiaux, T. E. Malliavin, and M. Nilges. Minimal NMR distance information for rigidity of protein graphs. *Discrete Appl. Math.*, 256:91–104, 2019. [doi:10.1016/j.dam.2018.03.071](https://doi.org/10.1016/j.dam.2018.03.071).

[27] C. Lavor, L. Liberti, N. Maculan, and A. Mucherino. The discretizable molecular distance geometry problem. *Computational Optimization and Applications*, 52:115–146, 2012. [doi:10.1007/s10589-011-9402-6](https://doi.org/10.1007/s10589-011-9402-6).

[28] C. Lavor, L. Liberti, and A. Mucherino. The interval branch-and-prune algorithm for the discretizable molecular distance geometry problem with inexact distances. *Journal of Global Optimization*, 56:855–871, 2013. [doi:10.1007/s10898-011-9799-6](https://doi.org/10.1007/s10898-011-9799-6).

[29] C. Lavor, A. Oliveira, W. Rocha, and M. Souza. On the optimality of finding DMDGP symmetries. *Computational and Applied Mathematics*, 40:1–10, 2021. [doi:10.1007/s40314-021-01479-6](https://doi.org/10.1007/s40314-021-01479-6).

[30] L. Liberti, C. Lavor, and N. Maculan. A branch-and-prune algorithm for the molecular distance geometry problem. *International Transactions in Operational Research*, 15(1):1–17, 2008. [doi:10.1111/j.1475-3995.2007.00622.x](https://doi.org/10.1111/j.1475-3995.2007.00622.x).

[31] L. Liberti, C. Lavor, N. Maculan, and A. Mucherino. Euclidean distance geometry and applications. *SIAM Review*, 56:3–69, 2014. [doi:10.1137/120875909](https://doi.org/10.1137/120875909).

[32] L. Liberti, B. Masson, J. Lee, C. Lavor, and A. Mucherino. On the number of solutions of the discretizable molecular distance geometry problem. In *Lecture Notes in Computer Science*, pages 322–342, Berlin, Heidelberg, 2011. Springer Berlin Heidelberg. [doi:10.1007/978-3-642-22616-8\\_26](https://doi.org/10.1007/978-3-642-22616-8_26).

[33] S. C. Lovell, I. W. Davis, W. B. Arendall, P. I. W. de Bakker, J. M. Word, M. G. Prisant, J. S. Richardson, and D. C. Richardson. Structure validation by  $\text{c}\alpha$  geometry:  $\phi$ ,  $\psi$  and  $\text{c}\beta$  deviation. *Proteins: Structure, Function, and Genetics*, 50(3):437–450, 2003. [doi:10.1002/prot.10286](https://doi.org/10.1002/prot.10286).

[34] T. E. Malliavin, A. Mucherino, C. Lavor, and L. Liberti. Systematic exploration of protein conformational space using a distance geometry approach. *Journal of Chemical Information and Modeling*, 59:4486–4503, 2019. [doi:10.1021/acs.jcim.9b00215](https://doi.org/10.1021/acs.jcim.9b00215).

[35] A. Mucherino, D. Gonçalves, L. Liberti, J.-H. Lin, C. Lavor, and N. Maculan. MD-jeep: a new release for discretizable distance geometry problems with interval data. In *Annals of Computer Science and Information Systems*, FedCSIS 2020. IEEE, sep 2020. [doi:10.15439/2020f35](https://doi.org/10.15439/2020f35).

[36] A. Mucherino, J.-H. Lin, and D. S. Gonçalves. *A Coarse-Grained Representation for Discretizable Distance Geometry with Interval Data*, pages 3–13. Springer International Publishing, 2019. [doi:10.1007/978-3-030-17938-0\\_1](https://doi.org/10.1007/978-3-030-17938-0_1).

[37] D. Nelson and M. Cox. *Lehninger Principles of Biochemistry: International Edition*. W.H.Freeman & Co Ltd, 2021.

- [38] C. Redfield. Proteins studied by NMR. In J. C. Lindon, G. E. Tranter, and D. W. Koppenaal, editors, *Encyclopedia of Spectroscopy and Spectrometry (Third Edition)*, pages 759–765. Academic Press, Oxford, third edition edition, 2017. [doi:10.1016/B978-0-12-803224-4.00089-3](https://doi.org/10.1016/B978-0-12-803224-4.00089-3).
- [39] Y. Shen and A. Bax. *Protein Structural Information Derived from NMR Chemical Shift with the Neural Network Program TALOS-N*, pages 17–32. Springer New York, 2015. [doi:10.1007/978-1-4939-2239-0\\_2](https://doi.org/10.1007/978-1-4939-2239-0_2).
- [40] R. Tavakoli and H. Zhang. A nonmonotone spectral projected gradient method for large-scale topology optimization problems. *Numerical Algebra, Control and Optimization*, 2(2):395–412, 2012. [doi:10.3934/naco.2012.2.395](https://doi.org/10.3934/naco.2012.2.395).